Table 1 Computational errors in different ranges[a]

Altitude range (ft)	Maximum error (% of true value)	Maximum error (ft and true value)	Comments
−1000 to 32,500	±0.021	+7.1 at 32,500	Error at zero altitude (reference) is −0.0023 ft Error is less than ±0.01% of true value throughout, for altitudes less than 31,000 ft
32,500 to 45,000	±0.026	+8.52 at 32,500	Error is less than ±0.01% of true value between 34,000 ft and 45,000 ft
45,000 to 60,000	±0.01	−4.82 at 48,000	At all other points the error is much less than ±0.01% of true value

[a] Computations are made for U.S. Standard Atmosphere Tables.[2]

proved the existing explicit relations for Mach number and airspeeds in the subsonic range for implementation in the on-board computers.

With a view to bringing the barometric altitude computation into a form similar to those obtained by Bogel, explicit equations involving only square root and summation operations have been obtained here. Logarithmic form of altitude computation is preferred when mechanical analog mechanisms are used. However, with the requirements for implementation on digital computer, the logarithmic form does not offer any particular advantage.

Because the basic relationship between altitude and the corresponding atmospheric pressure is an exponential one, in general the altitude can be expressed as a power series. The power series can be either in terms of atmospheric pressure p itself, or in terms of the ratio of atmospheric pressure p to the reference standard mean sea-level pressure p_0. The latter case is required in the lower altitude ranges for landing purposes. Thus, it is possible to find an equation of the form

$$h = a + [b + cy + d(y)^{1/2}]^{1/2} \tag{1}$$

where h is the altitude to be computed, a, b, c, and d are constants, and y is either pressure or pressure ratio. For the purposes of computation, the altitude range of −1000 ft to +60,000 ft is divided into three overlapping ranges. Four suitable points were chosen in each range and the simultaneous equations were solved to obtain the values of a, b, c, and d in each range. The equations so obtained are

$$h_1 = 10.5323 - [-11.1767 - 5.5179y + 127.6249(y)^{1/2}]^{1/2} \times 10^4 \text{ ft} \tag{2}$$

for $-1000 \text{ ft} \le h_1 \le 32{,}500$ ft

$$h_2 = 7.4599 - [-13.6337 + 0.5633p + 9.5546(p)^{1/2}]^{1/2} \times 10^4 \text{ ft} \tag{3}$$

for $32{,}500 \text{ ft} \le h_2 \le 45{,}000$ ft, and

$$h_3 = 12.3836 - [-20.4965 - 3.941p + 47.8316(p)^{1/2}]^{1/2} \times 10^4 \text{ ft} \tag{4}$$

for $45{,}000 \text{ ft} \le h_3 \le 60{,}000$ ft where $y = p/p_0$.

The errors in values of altitudes computed with these equations are shown in Table 1. The accuracy requirements for pressure altitude, as specified in ARINC Characteristic No. 545, range from ±2.5% to ±0.25% for different altitudes up to 60,000 ft. From Table 1, it is evident that the Eqs. (2-4) give required accuracy for computational purposes. The particular division of ranges i.e., −1000 ft to +32,500 ft, 32,500 ft to 45,000 ft, and 45,000 ft to 60,000 ft is done to keep the computational errors within the required limits. However, ranges can be extended with loss in accuracy. For example

$$h_4 = 10.5271 - [-11.1656 - 5.5124y + 127.4973(y)^{1/2}]^{1/2} \times 10^4 \text{ ft} \tag{5}$$

in place of Eq. (1), would cover a range from −1000 ft to +39,000 ft with an error less than ±0.05% of true value.

It can be observed that with these equations no particular distinction is made in computations at tropopause transition level. The equations are simply fitted to U.S. Standard Atmosphere values and the measured values of pressure require usual corrections. It is not claimed that the implementation of these equations would offer many advantages especially with advanced digital computation techniques now available, but these equations go well with the equations for Mach number and airspeeds in the forms proposed by Bogel.

References

[1] Bogel, W., "Explicit Approximate Equations for Calculating Mach Number and Various Airspeeds," European Space Research Organization, Oberpfaffenhofen, West Germany, ESRO TT-100, Oct. 1974.

[2] Herrington, R.M., Shoemaker, P.E., Bartlett, E.P., and Dulap, E.W., "Flight Test Engineering Handbook," Air Force Systems Command, Air Force Flight Test Center, Edwards Air Force Base, Calif., TR 6273, Jan. 1966.

Aerodynamic Heat Transfer to a Hypersonic Research Aircraft Model (X-24C) at Mach 6

Pierce L. Lawing* and James L. Hunt†
NASA-Langley Research Center, Hampton, Va.

Introduction

A joint USAF/NASA study has developed a conceptual design for a new high-speed research airplane (X-24C).[1] The vehicle, a rocket-boosted, delta planform aircraft, is launched from a B-52 and is capable of 40 sec of rocket cruise

Received June 28, 1976

Index categories: Boundary Layers and Convective Heat Transfer—Turbulent; aircraft Testing (including Component Wind Tunnel Testing); Aircraft Configuration Design.

*Aero-Space Technologist, Aerodynamic Analysis Section, High-Speed Aerodynamics Division. Member AIAA.

†Head, Aerodynamic Analysis Section, High-Speed Aerodynamics Division. Member AIAA.

at Mach 6 ($q = 1000$ psf, $R_{\infty,L} = 55 \times 10^6$) with a research scramjet. Research provisions include a 10-ft-long experiments section, removable fins and strakes, and configuration geometry for testing integrated air breathing propulsion systems.

Heat-transfer tests were conducted on a 1/29-scale model of the X-24C-121 configuration in the Langley Mach 6, 20-in. tunnel at a Reynolds number of 13×10^6 using the phase-change heat-transfer technique.[2] This note presents some results from the experimental study.

Configuration

The configuration, slightly modified from the baseline configuration of Ref. 1, has a flat-bottom forebody to the scramjet engine attachement, and the fuselage sides are also flat except for a bulge at the canopy location. The wings have a flat-bottom surface with a 68 deg leading edge sweep angle and 30 deg dihedral angle. To obtain a maximum amount of data with a minimum of testing, the model had asymmetric deflections of the elevons, center-fin drag brakes, and body side fin toe-in.

Results and Discussion

The results are partially presented in terms of phase-change heat-transfer patterns (Figs. 1 and 3). The nominal heat-transfer coefficient ratios given for each pattern apply to the interface between the melted (dark) and unmelted (white) regions. The h_s parameter used to nondimensionalize the data is the laminar heat-transfer coefficient at the stagnation point of a 1-ft radius sphere at the model scale (1/29) and the tunnel conditions. For the data presented here, h_s has a nominal value of 0.047 BTU/ft-sec°R (960.21 W/m^2°K). Coefficients for the phase-change isotherms are presented for both laminar $(h/h_s)_L$ and turbulent $(h/h_s)_T$ nominal adiabatic wall-to-total temperature ratios of 0.85 and 0.92, respectively.

Windward Side Heating

A sequence (taken from one tunnel test) of phase-change heat-transfer pattern photographs on the windward side (bottom) of the configuration for a Reynolds number of 13×10^6 is presented in Fig. 1 for an angle of attack of 4 deg. The first photograph of the sequence shows that the phase-change has occurred on the nose tip and on the outboard position of the 10 deg windward-deflected elevon. The second photograph shows an unexpected phenomenon. Melt not only has occurred on the leading edges, but inboard along strips roughly parallel to the leading edges. The third photograph shows transition to fully turbulent flow on the wings and a "cold streak" on the forebody centerline. The final photograph indicates the level of heating typical of a large percentage of the windward forebody. Oil flow patterns indicate a region of very low shear (similar to a separation bubble) in the unmelted region just downstream of the apex. The unusual forebody heating pattern (parallel to the forebody leading edge) in the second photograph is assumed to be the end of transition to turbulent flow (oil flow patterns indicate a turning of the flow along the more upstream interface toward a less inward direction). The transition is the result of cross flow due to the blunt leading edge flow, and the "cold streak" on the forebody centerline is assumed to be the result of a thickened boundary layer due to the inward residual crossflow and the symmetry of the model.

Windward side phase-change patterns were also obtained with increasing angle of attack ($\alpha = 4$, 8, 12, and 16 deg). At

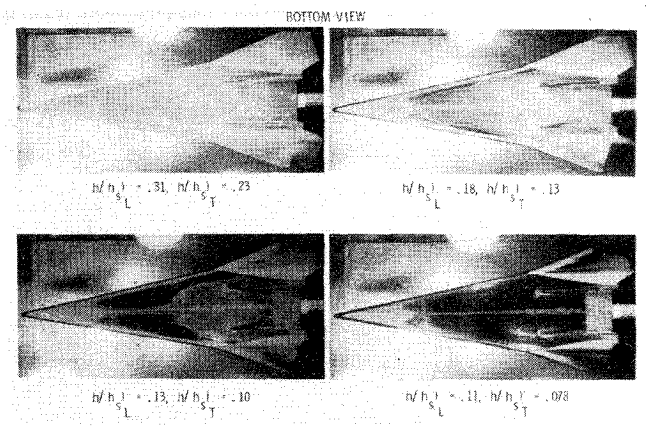

Fig. 1 Phase-change heat transfer patterns on X-24C-121 model at Mach 6, $\alpha = 4$ deg, $R_{e,L} = 13.0 \times 10^6$, $h_s = 0.0470$ BTU/ft^{2}sec°R.

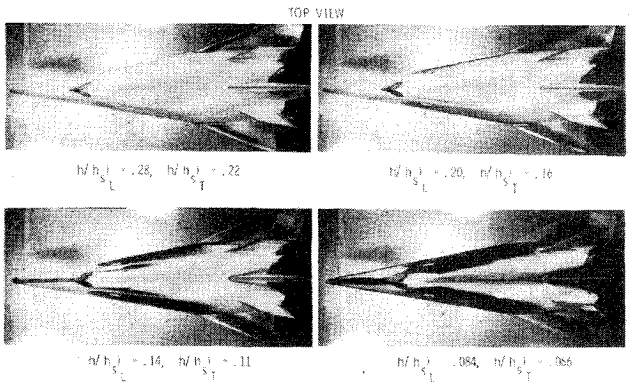

Fig. 3 Phase-change heat-transfer patterns on X-24C-121 model at Mach 6, $\alpha = 4$ deg, $R_{e,L} = 13.0 \times 10^6$, $h_s = 0.0469$ BTU/ft^{2}sec°R.

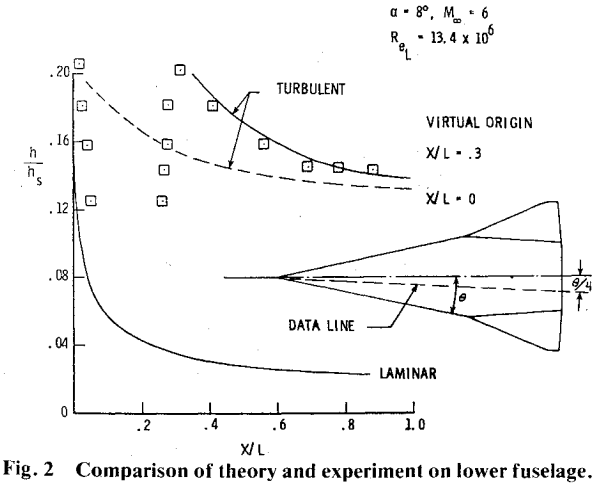

Fig. 2 Comparison of theory and experiment on lower fuselage.

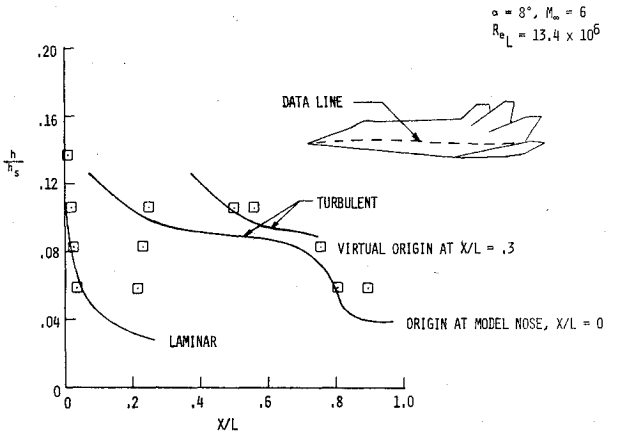

Fig. 4 Comparison of theory and experiment on fuselage side.

an angle of attack of 8 deg the pattern is similar to that at $\alpha = 4$ deg, that is, the "cold streak" along the centerline is still present. At angles of attack of 12 and 16 deg the forebody windward heating is similar to that which occurs on a delta wing at high angle of attack.[3]

Figure 2 is a comparison of data and theory on the fuselage bottom at an angle of attack of 8 deg, along a data line which passes through the turbulent area. The theories shown utilize the T' method for laminar heating and the Spaulding-Chi method as modified by Neal and Bertram[4] for turbulent values. The Hypersonic Arbitrary Body Program,[5] modified to provide the heat transfer information, generated the boundary layer edge conditions using the tangent cone approximation. The turbulent heating theory has been shifted by assuming that the end of transition was equivalent to a new sharp leading edge or virtual origin. This location was determined from the earliest melt (or highest heating) of the region assumed to be turbulent. As shown in Fig. 2, the two theories bracket the data and the turbulent theory starting from a virtual origin location of $X/L = 0.3$ gives good agreement with the data.

Leeside Heating

A sequence of phase-change patterns on the leeside at an angle of attack of 4 deg is shown in Fig. 3. The first photograph of the sequence shows transition from laminar to fully turbulent flow on the wing and melted regions (high heating rates) on the canopy and leading edges. In the second photograph, melt is occurring on the sides along a line just inboard of the fuselage leading edge (note that the heating level here is comparable to that on the canopy and the leading edges). The third photograph indicates the extent of the high heating rates on the sides along with the interference heating downstream of the canopy, at the wing root, center-vertical tail/fuselage juncture and upstream of the drag brakes, as well as the leading-edge heating upstream of the canopy. The salient feature in the final photograph is the interference heating along the leeward centerline produced by the vortex which begins aft of the canopy.

The data along the fuselage side are compared with theory in Fig. 4 for $\alpha = 8$ deg. Again, the agreement between data and the prediction method is reasonably good.

Concluding Remarks

The Hypersonic Arbitrary Body Program (HABP) in conjunction with accepted, easily used heat-transfer prediction techniques has been shown to give reasonably good overall agreement with experimental results and is a reasonable way to predict the type of heating information needed to generate nominal thermal protection system weights. The phase-change paint technique gives easily interpreted graphic indication of local areas not covered by assumptions of the analytic technique along with the heating level to allow detail corrections to the thermal protection system. The paint technique also allows a rapid check of the heating level over the large areas of the test model.

References

[1] Kirkham, F.S. and Jones, R.A., "Joint USAF/NASA Hypersonic Research Aircraft Study," AIAA Paper 75-1039, Anaheim, Calif., Aug. 1975.

[2] Jones, R.A. and Hunt, J.L., "Use of Fusible Temperature Indicators for Obtaining Quantitative Aerodynamic Heat-Transfer Data," NASA TR R-230, Feb. 1966.

[3] Johnson, C.B. "Boundary-Layer Transition and Heating Criteria Applicable to Space Shuttle Configurations from Flight and Ground Tests," presented at NASA Space Shuttle Technology Conference; Volume I—Aerothermodynamics, Configurations, and Flight Mechanics," NASA TM X-2272, April 1971.

[4] Neal, L., Jr. and Bertram, M.H., "Turbulent-Skin-Friction and Heat-Transfer Charts Adapted from the Spaulding-Chi Method," NASA TN D-3969, 1967.

[5] Gentry, A.E. and Smyth, D.C., "Hypersonic Arbitrary-Body Aerodynamic Component Program (Mark III Version)," Vol. II—Program Formulation and Listings," Rep. DAC 61552, Vol. II—(Air Force Contract Nos. F3361 67 C 1008 and F33615 67 C 1602), McDonnell Douglas Corporation, April 1968 (available from DDC as 851 812).

Aerodynamics of Sideslipping Delta Wings at Incidence with Leading-Edge Separation

M.J. Cohen*
The Technion, Israel Institute of Technology, Haifa, Israel

Nomenclature

p = rolling speed, $\bar{p} = ps/V\epsilon$
s = local semispan of delta wing
s_o = local semispan of delta wing at pitch axis, $\bar{s_o} = s_o/s$
U = relative wind velocity
x,y = coordinates in Z-plane, $Z = x + iy$
$\bar{Z}$ = Z/s, $\bar{Z} = \frac{1}{2}(\xi + 1/\xi)$
C_p = pressure coefficient, $C_p = p/(\frac{1}{2}\rho U^2)$
C_L = normal force coefficient, $C_L = L/(\frac{1}{2}\rho U^2 S)$
C_l = rolling moment coefficient about body axis in the plane of symmetry of the wing, $C_l = \ell/(\frac{1}{2}\rho U^2 Ss)$
α = angle of incidence, $\bar{\alpha} = \alpha/\epsilon$
β = angle of sideslip, $\bar{\beta} = \beta/\epsilon$
Γ_i = vortex core strength
ϵ = semiapex angle of delta wing
θ = polar angle defined by $y = s\cos\theta$
ρ,σ = polar coordinates of a point in the ξ-plane, $\xi = \rho e^{i\sigma}$
σ_i = angular location of vortex cores in the ξ-plane,
ξ = $\rho e^{i\sigma}$, $\bar{\xi} = 2\xi/s = \bar{\rho} e^{i\sigma}$, $\bar{\xi} = \bar{Z} + (\bar{Z}^2 - 1)^{\frac{1}{2}}$
i = 1,2: subscripts relating quantities to windward and leeward isolated vortices, respectively

Introduction

UPON consideration of previous work by D. Nimri and the author,[1] it became evident that the solution of the problem of the slender delta wing in sideslip and in separated flow could be obtained as a derivative of the more general solution presented in that reference. The desirability of describing here that special solution was reinforced by the then lack of existing theoretical work on the subject, coupled with the realization that it would afford a useful, approximate, closed-form solution to a problem of practical concern. It was only after this task was accomplished that the author became aware that Pullin[2] had recently obtained numerically developed solutions for the same problem. In view of the simplicity of the closed-form expressions for the aerodynamic coefficients which are derived in the sequel, it has been decided to present these nonetheless and to test some of the results against (1) Pullin's results in the practical parametral $(\bar{\alpha},\bar{\beta})$ range, and (2) Harvey's[3] experimental data for specific wings operating under conditions covered by both methods. Furthermore, the range of applicability of the present method includes the low-incidence $(\bar{\alpha} \leq 0.5)$ subrange, in parts of which $(\bar{\beta} \geq 1.0)$ Pullin's numerical procedure fails to yield a solution.

Received Feb. 2, 1976; revision received May 26, 1976.
Index category: Aircraft Aerodynamics (including Component Aerodynamics).

*Associate Professor, Department of Aeronautics. Member AIAA.